Nonlinear elasticity of single collapsed polyelectrolytes

Hirofumi Wada,* Yoshihiro Murayama, and Masaki Sano
Department of Physics, University of Tokyo, Hongo, Tokyo, 113-0033, Japan
(Received 6 January 2005; revised manuscript received 14 June 2005; published 10 October 2005)

Nonlinear elastic responses of short and stiff polyelectrolytes are investigated by dynamic simulations on a single-molecule level. When a polyelectrolyte condensate undergoes a mechanical unfolding, two types of force-extension curves—i.e., a force plateau and a stick-release pattern—are observed depending on the strength of the electrostatic interaction. We provide a physical interpretation of such force-extension behavior in terms of intramolecular structures of the condensates. We also describe charge distributions of counterions condensed onto a polyelectrolyte, which clarify formation of one-dimensional strongly correlated liquid at large Coulomb coupling regime. These findings may provide significant insights into the relationship between a molecular elasticity and a molecular mechanism of like-charge attractions observed in a wide range of charged biopolymer systems.

DOI: 10.1103/PhysRevE.72.041803 PACS number(s): 61.20.Qg, 82.35.Rs, 87.15.He

I. INTRODUCTION

Electrostatic interactions in aqueous media can be controlled by changing the temperature, dielectric constant of the solvent, and counterion valency [1]. It is well known that the celebrated Poisson-Boltzmann (PB) or Debye-Hueckel theory provides a good description of a weakly charged or high-temperature system for which the mean-field approximation works well [1,2]. In a strongly charged system, however, effects of correlations between counterion charge fluctuations, which are neglected within the widely used PB theory, give rise to several unexpected phenomena [3–21]. Especially in biological systems, macromolecules such as polynucleic acids, proteins, and membranes, which are all dissolved in water containing various salt ions and usually carry their large number of charges, electrostatic interactions often play a central role in determining the phase behavior of such systems. Among them, one of the most familiar examples is the condensation of a single DNA molecule in the presence of various polyvalent cations [22–26]. DNA is a highly negatively charged polymer with the elementary charge unit $-e$ per 0.17 nm. DNA-DNA interactions in aqueous solution with physiological condition (0.14*M* NaCl plus possible other ions) are therefore modeled as screed Coulomb repulsive interactions with a Debye-Hueckel screening length of $\lambda_D \sim 1$ nm. The addition of a small amount of polyvalent cations—e.g., spermidine—however, leads to the compaction of a single DNA molecule to specific structures, such as a toroid or rod. Even a densely packed DNA condensate still has a net negative charge; this compaction is often termed as a counterintuitive "like-charge attraction." Thanks to a huge amount of theoretical, numerical, and also experimental studies in these two decades [3–29], the equilibrium properties of like-charge attraction are now becoming clear.

On the other hand, ionic effects coming from counterion degrees of freedom also modify the elasticity of a polyelectrolyte (PE) chain [30–35]. Recent micromanipulation experiments have shown impressive elastic responses of single DNA molecules collapsed by polyvalent cations [36–38], which significantly deviate from the entropic elasticity of an ideal wormlike chain (WLC) [39]. For a relatively low concentration of spermidine, the measured force curve has a plateau in a wide range of the polymer's extension, which has been typically seen in pulling a polymer globule [40]. With increasing the concentration of spermidine, the compaction of DNA becomes stronger, leading finally to the appearance of a striking sawtooth pattern in its force-extension curve, which is specifically called as a "stick-release pattern." This type of periodic response can be attributed to turn-by-turn unfolding of toroidal supercoiling [38,41], though any direct evidence of that is not yet available. What is important in those experiments is that the PE's mechanical responses to applied large deformations not only reflect the PE's equilibrium condensate structure, but also involve dynamic effects. The experimental finding thus offers a combined problem of long-ranged Coulomb and nonequilibrium effects, which makes this problem highly complicated. In spite of that clear experimental evidence, therefore, there exist a few theoretical and numerical studies on this and related problems so far [42–46]; our understanding seems at present far from satisfactory.

In this paper, we report results of a Brownian dynamics (BD) simulation of the stretching of single PE condensates. The present simulation covers only a salt-free system with a short chain strand as a first step, but effects of counterions which are strongly coupled to PE's are taken into account explicitly. The force-extension (f-x) curve of a PE chain shows WLC entropic elasticity, a force plateau, and a stick-release-like pattern as the electrostatic coupling increases. This trend is consistent with that observed in DNA stretching experiments [36–38], where the electrostatic coupling strength is controlled by the concentration of added polyvalent cations. Note that, experimentally, the effective charge valency of counterions nearby a PE, which controls the strength of the electrostatic effect to thermal energy, increases with an increase of the concentration of added polyvalent cation, due to the entropically driven counterion exchange between monovalent and polyvalent cations [47]. By

*Present address: Physik Department, Technical University Munich, 85748 Garching, Germany. Electronic address: wada@ph.tum.de

investigating the charge ordering of counterions for both condensed and unraveled PE's, we find that counterions are in a fluid phase with moderate correlations for a force-plateau case, while they possess a short-range ionic crystal-like order with strong correlations for the stick-release case. In order to highlight electrostatic effects upon PE's mechanical properties, we are primarily focusing on systems with very strong Coulomb interactions which are beyond typical physiological conditions. Furthermore, the present study deals only with relatively short and stiff polymers and also neglects complicated structures of biopolymers [48]; a direct comparison with any experiment may be impossible at this stage. The primary aim in this work is to build bridges between the single-molecule elasticity and the physical pictures of the counterion-induced attractions from the dynamical perspective, which may serve as a first step towards achieving a microscopic understanding of available experiments.

This paper is organized as follows. In the next section, we set up our dynamic simulation model and describe the numerical details with some additional remarks. In Sec. III, the effective persistence length of PE is deduced from its force-extension curve for a swollen (uncondensed) PE, and its dependence upon the electrostatic effect is discussed in terms of the counterion condensation onto the PE. In Sec. IV, the charge-ordering behavior inside a PE condensate is investigated for large coupling regimes, where ionic pairings between PE monomers and counterions are clarified. Section V provides force-extension curves of PE condensates in the strong-coupling regime, which are also interpreted in terms of PE's intrachain behavior under stretching. In Sec. VI, we describe counterion distributions along stretched PE's, together with the influence of the pulling speed upon force-extension curves. Our conclusion and perspective are given in the last section.

II. MODEL

In our BD simulation, the chain comprises N harmonically linked beads of radius a, each of which carries a charge $-qe$. The system also includes N oppositely charged counterions of the same valency and radius to keep the overall charge neutrality [49,50]. The charged particles interact via the unscreened Coulomb interaction, where the solvent is replaced by a background with the dielectric constant ε. The system is placed in a cubic box, and periodic minimum-image boundary conditions are imposed to keep the monomer and counterion density $\rho_{mon}=\rho_{ion}\approx 1.5\times 10^{-5}/a^3$ constant [51–53]. The long-time dynamics of monomers and counterions is described by the position Langevin equation [54,55]

$$\gamma\frac{d\mathbf{r}_i}{dt}=-\nabla_{\mathbf{r}_i}U[\mathbf{r}(t)]+\mathbf{f}_i(t), \tag{1}$$

where γ is the damping constant, U the potential energy, and $\mathbf{f}_i$ the vectorial random force acting on the particle i, which satisfies the correlation property $\langle\mathbf{f}_i(t)\mathbf{f}_j(t')\rangle=2\gamma k_BT\delta_{ij}\mathbf{1}\delta(t-t')$. Hydrodynamic interactions between any particles are not taken into account in this study.

The potential energy is composed of several kinds of contributions: $U=U_s+U_b+U_c+U_{LJ}$. The first one U_s, of the form

$$U_s=\sum_{i=1}^{N-1}\frac{K}{2}(|\mathbf{r}_{i+1}-\mathbf{r}_i|-b)^2, \tag{2}$$

ensures the connectivity of a PE with the bond length b. To maintain small variances of bond lengths around b, or the chain length around $L=b(N-1)$, we use a large value of the spring constant, $K=400\epsilon_{LJ}/a^2$, where ϵ_{LJ} is the energy scale of the Lennard-Jones potential shown below. The second one U_b accounts for the intrinsic bending stiffness of a PE backbone, which we set as

$$U_b=\sum_{i=1}^{N-2}\kappa(1-\hat{\mathbf{u}}_i\cdot\hat{\mathbf{u}}_{i+1})=\sum_{i=1}^{N-2}\kappa(1-\cos\theta_i), \tag{3}$$

where κ is the bending constant, $\mathbf{u}_i=\mathbf{r}_{i+1}-\mathbf{r}_i$ the bond vector, and $\hat{\mathbf{u}}_i=\mathbf{u}_i/|\mathbf{u}_i|\cong\mathbf{u}_i/b$ and where θ_i is the bond angle between consecutive bonds $\mathbf{u}_i$ and $\mathbf{u}_{i+1}$. The bare persistent length is thus given by $L_p^0=b\kappa/k_BT$. The Coulomb potential U_c acts between all charged particles except between bonded ones, which is given by

$$U_c=\frac{q^2e^2}{4\pi\varepsilon}\sum_{i>j}\frac{s_is_j}{|\mathbf{r}_i-\mathbf{r}_j|}, \tag{4}$$

where $s_j=\pm 1$ stands for the sign of the charge. Last, in order to prevent a collapse of monomers and counterions, a purely repulsive Lennard-Jones potential U_{LJ} acting between all particles is also incorporated,

$$U_{LJ}=\epsilon_{LJ}\sum_{i<j}\left(\frac{b^{12}}{|\mathbf{r}_i-\mathbf{r}_j|^{12}}-2\frac{b^6}{|\mathbf{r}_i-\mathbf{r}_j|^6}+1\right), \tag{5}$$

only for $|\mathbf{r}_i-\mathbf{r}_j|<b$.

The particle radius a, the L-J energy scale ϵ_{LJ}, and the associated diffusive time $\tau=\gamma a^2/\epsilon_{LJ}$ are chosen as the unit of length, energy, and time in our simulation. In rescaled units, the coupling constant $\Gamma=q^2\ell_B/a$ controls the relative strength of the electrostatic interaction to the thermal energy at a distance a. (The Bjerrum length $\ell_B=e^2/4\pi\varepsilon k_BT\approx 0.7$ nm in water at room temperature.)

In the beginning of our simulation, a polymer with a randomly generated initial configuration is allowed to collapse to a globule and is equilibrated for 5×10^6–10^7 time steps with $\Delta t=0.001\tau$. A condensed PE is then stretched by pulling its one end at a constant speed, while the other end is fixed in a position. In all simulations presented below, we fix $N=32, b=2a$, $L/L_p^0=4$, and $k_BT=0.3\epsilon_{LJ}$, unless otherwise stated, while Γ is changed from 0 up to 110. The long-run data for $N=64$ is also shown briefly. For a single stretch-relax cycle, simulation runs for 10^8–10^9 time steps for $N=32$. Simulations for larger N systems, which are much more time consuming, are currently underway.

The choice of the pulling speed is a delicate problem, since the unfolding of a condensed PE is nonequilibrium. In the present study, the pulling speed v_s is given in units of $v_0=b/\tau_R$, with $\tau_R=\gamma b^2N^2/3\pi^2\epsilon_{LJ}$ being the Rouse relaxation

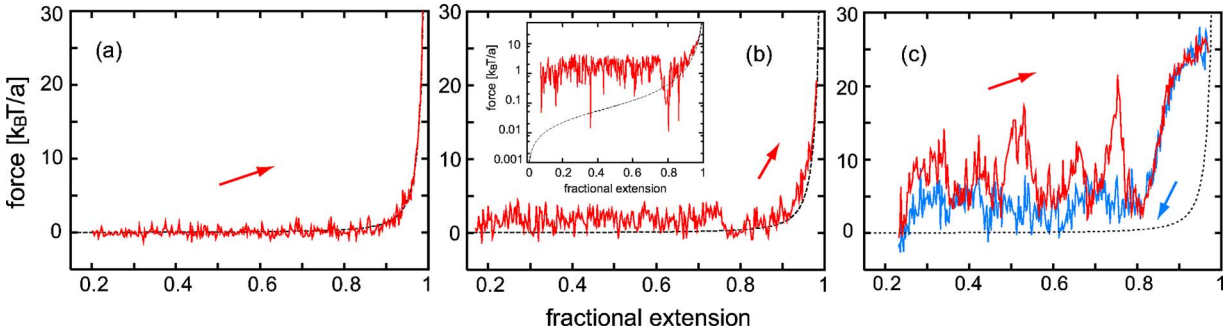

FIG. 1. (Color online) The force-extension curves of a PE for three different values of the coupling parameter (a) $\Gamma=0.1$ (WLC), (b) $\Gamma=40$ (force plateau), and (c) $\Gamma=110$ (stick release). The dashed lines are Eq. (6) with bare persistence length L_p^0 as a reference. Arrows indicate stretching (red) and relaxing (blue). In the inset of (b), points with negative force values are removed.

time for a flexible polymer with N monomers at $k_BT=\epsilon_{LJ}$ [54,55]. This is just a tentative choice, and we fix $v_s=0.1v_0$ throughout this paper. In Sec. VI we will demonstrate that this pulling speed is slow enough to minimize the pulling-rate dependence on force curves by systematically investigating how the behavior of f-x curves are affected by the increase of v_s.

Some remarks are in order. The elastic potential, Eq. (3), works well only for small θ (i.e., a linear response regime). For a large local bending of the chain (over the angle $\pi/2$), it decreases its energetic penalty, which is obviously unphysical. However, for its simplicity, we use Eq. (3) throughout this study, regardless of the magnitude of Γ. We therefore set a relatively large L_p^0 to avoid any artificial effect, and actually as shown below, our result in this paper is free from an unphysical effect caused by a local large deflection of the bond angle. For a longer PE, however, other types of potential form, such as $(1-\cos\theta)^2$ or $\kappa_1\theta^2+\kappa_2\theta^4$, where κ_1 and κ_2 are positive constants, would be better [25,56,57].

The use of the periodic minimum-image condition automatically set the large-distance cutoff R_c, which is half the box length, for any interparticle interactions. Because of the long-ranged nature of the Coulomb interaction, each charged particle interacts not only with all others within the central simulation box, but also with its all periodic images in principle. This implies the absence of a cutoff length in Coulomb systems; more precise computational methods are better [49,50]. The introduction of the cutoff R_c, however, is not problematic in the present study for the following reasons. For large Γ, most of the counterions condense onto a PE, which indicates that a PE complex is almost charge neutral, especially when it collapses. Because each box contains a PE in a very dilute condition, Coulomb interactions with periodic images are expected to be vanishingly small. For the opposite case where counterions are expanded over the box, the Coulomb interaction is expected to be sufficiently weak to be also safely neglected beyond the cutoff distance.

At the present stage, we neglect the hydrodynamic interactions between any particles. For a globular PE, this is not a serious drawback, because inside the globule, hydrodynamic interactions are significantly screened [54,55] and are also overwhelmed by large Coulomb forces. However, an intrachain structure of a PE condensate can be affected by its folding kinetic pass (since in BD simulations it approaches its ground state only very slowly), where a hydrodynamic interaction plays a crucial role. Also, counterion motions on an extended PE are affected by their hydrodynamic interactions in some way. Incorporating a hydrodynamic interaction properly in this system remains our future study.

III. COUNTERION CONDENSATION

Figure 1(a) shows the f-x curve of the PE for $\Gamma=0.1$. Because of the almost unscreened Coulomb interactions between PE monomers, the PE is substantially swollen. The f-x curve thus obeys the WLC interpolation formula given by

$$\frac{L_p f_0}{k_B T} = u + \frac{1}{4(1-u)^2} - \frac{1}{4}, \tag{6}$$

where $u=x/\langle L\rangle$ is the fractional extension of a PE [39]. The effective persistence length L_p in Eq. (6) is now Γ dependent. To see this feature systematically, we plot in Fig. 2 the effective L_p as a function of Γ. They are determined by fitting Eq. (6) to the simulated f-x curves for $0.80\leqslant u\leqslant 0.98$. For small Γ (roughly less than 3), the electrostatic repulsion between monomers leads to a stretched configuration of the PE—i.e., an increasing stiffness. As Γ further increases beyond the onset value of the Manning condensation $\Gamma_c\approx 2$ (for an infinitely long, stiff chain [58]), net repulsions be-

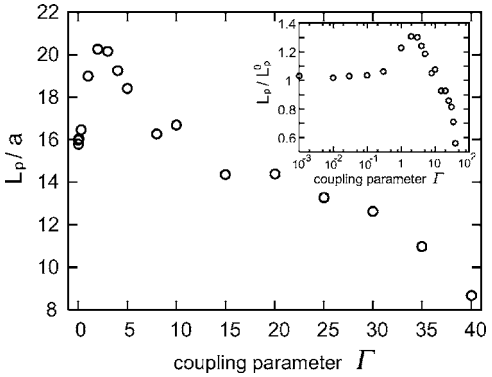

FIG. 2. The effective persistence length L_p of a PE estimated from its force-extension curve as a function of Γ. The inset is the same plot for L_p/L_p^0 on a semilogarithmic scale.

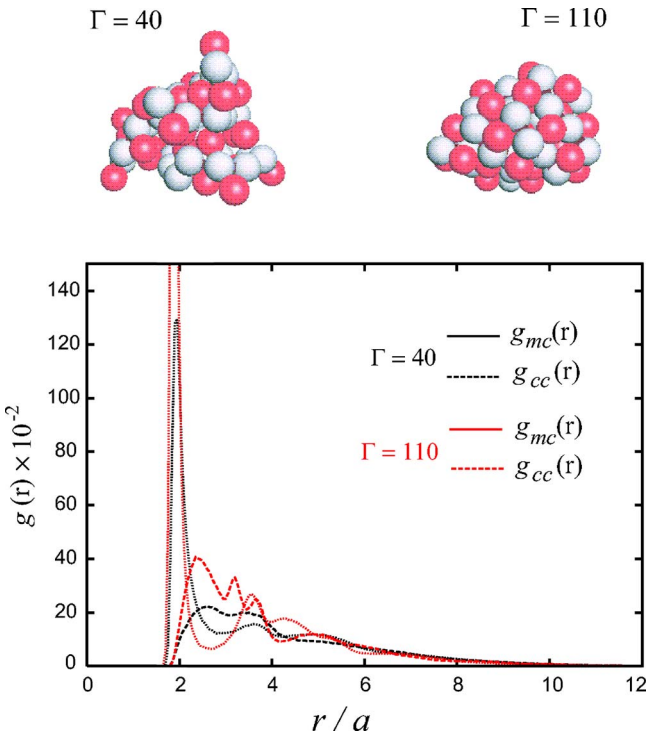

FIG. 3. (Color online) Top: snapshots of the PE condensates for $\Gamma=40$ and $\Gamma=110$ at time steps 1.2×10^7. Bottom: (angle-averaged) pair-distribution functions of monomer and counterion, $g_{mc}(r)$ (straight line), and of two counterions, $g_{cc}(r)$, (dashed line) for $\Gamma=40$ (black) and for $\Gamma=110$ (red).

tween PE monomers are more and more screened out by the counterion condensation, leading thereby to a significant reduction of L_p. The behavior is consistent with that of the radius of gyration, R_g, for a stress-free PE observed in other simulations [51–53], if one recalls that the persistence length is related to the radius of gyration as $R_g^2\sim 2L_pL$ for a (neutral) semiflexible polymer. For $\Gamma>20$, L_p becomes smaller than L_p^0, which implies a (long-ranged) net attraction between PE monomers, due to the Coulombic instability [59]. Around the transition point, data dispersion of L_p is remarkable, while the precise critical value of Γ is at present unclear because of significant finite-size effects.

IV. PE CONDENSATES AND CHARGE ORDERING

For a sufficiently large Γ, a stress-free PE condenses into a compact form. Figure 3 shows snapshots for $\Gamma=40$ and 110 at time steps $t=1.2\times10^7$, respectively. Both cases are above their crystallization point; the PE for $\Gamma=110$ is much more tightly packed. Figure 3 also shows the pair-distribution functions of monomers and counterions, $g_{mc}(r)$, and between counterions, $g_{cc}(r)$. They are together given by

$$g_{\alpha\beta}(r)=\frac{1}{N}\left\langle\sum_{i,j}\delta(\mathbf{r}-\mathbf{r}_i^{\alpha}+\mathbf{r}_j^{\beta})\right\rangle-\delta(\mathbf{r})\,\delta_{\alpha\beta}, \tag{7}$$

where we assume a spherical symmetry for a PE condensate. One can find in Fig. 3 a pronounced peak at $r\approx 2a$, which indicates that monomers and counterions are binding strongly; i.e., they are making ionic pairs. $g_{cc}(r)$ for $\Gamma=40$ suggests that the counterions form a certain short-range structure due to their mutual correlations, but as well its peaks are overlapped and are rather broad. This is because, although the condensed counterions are moderately correlated, they are in a fluid phase due to significant thermal fluctuations. On the other hand, there can be seen a few distinct peaks in $g_{cc}(r)$ for $\Gamma=110$, confirming that the counterions possess a clear short-range order, analogous to an ionic crystal.

V. FORCE PLATEAU

For $\Gamma=40$ a force plateau appears in the f-x curve, which can be most clearly seen in the semilog arithmetic plot of inset in Fig. 1(b). The magnitude of the condensation force between PE monomers is the quantity that can be compared with those of experiments. The excess work defined by

$$\Delta W=\int_{x_1}^{x_2}(f-f_0)dx=\bar{f}(x_2-x_1) \tag{8}$$

is calculated from the data, where f_0 is the WLC force of Eq. (6) and where x_1 and x_2 are set to $0.3\langle L\rangle$ and $0.8\langle L\rangle$. We obtain $\Delta W\sim 0.8k_BTL/a$, which corresponds to $\bar{f}\sim 3.2k_BT$ per monomer. Since this attractive force can be overwhelmed by a disturbing thermal fluctuation of a few k_BT, fluctuation effects of monomers and counterions are still important for this Γ. The net attraction here, which is coming from fluctuating dipole-dipole interactions and is thus purely electrostatic origin, is known to be an increasing function of Γ [14]. Let us therefore tentatively compare our $\bar{f}/\Gamma$ with that of available experiment having a different value of Γ. Assuming DNA's linear charge density $\nu=q/(2a)$ and the charge valency $q=4$ in our model, we have $a\sim 0.34$ nm (1 bp), which gives $\bar{f}/\Gamma\sim 0.04k_BT/\mathrm{bp}$ for $\Gamma=40$. On the other hand, for DNA with trivalent cation ($q=3$) at room temperature, one finds $\Gamma=2\nu l_B/a\cong 24$. Using the experimental value $\Delta W=0.33k_BT/\mathrm{bp}$ for trivalent cation CoHex obtained by Baumann *et al.* [36], one finds $\bar{f}/\Gamma\sim 0.01k_BT/\mathrm{bp}$ for $\Gamma=24$, which agrees with our value.

Snapshots of the PE during stretching for $\Gamma=40$ are displayed in Fig. 4. Here, all the counterions condense onto the PE; i.e., the charge of the PE is completely neutralized. At the intermediate stage of the pulling, the so-called ball-chain configuration is found. (See also Fig. 5.) Note that the origin of the ball-chain structure here is entirely different from that of the PE in a bad solvent. Because attractions are not so strong (typically a few k_BT as revealed above), the PE condensate can change the intrachain conformation to minimize the stored elastic energy according to externally applied deformation. The deformation of the PE globule thus requires only constant pulling force.

Figure 5 shows the variation of the number of monomers remaining in the globular object N_g, as a function of the extension x. As is clearly seen, N_g linearly decreases with x, directly indicating that the number of unfolded monomers, $N-N_g$, linearly increases with x. It is important to note that

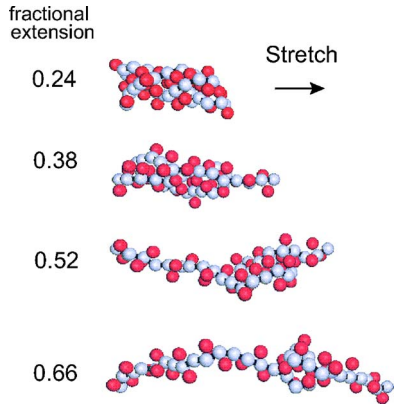

FIG. 4. (Color online) Snapshots of a PE under stretching for $\Gamma=40$. Corresponding f-x curve is Fig. 1(b). Red and white spheres represent counterions and monomers, respectively. All the counterions are condensed onto the PE.

this is exactly corresponding to the force-plateau stage in Fig. 1(b). The finding is simply understood as follows [60,63]. For a typical ball-chain configuration (as schematically shown in Fig. 5), the flexibility, or the entropic elasticity, is governed by the unfold monomers, because inside the globule, monomers tightly stick with each other and hardly move. Introducing thereby the PE's effective contour length L_{eff}, the tensile force f might be given by Eq. (6) with the replacement of the original contour length L by the effective one, L_{eff} [63]. Since Eq. (6) contains x and L_{eff} solely in the fractional form x/L_{eff}, approximately constant x/L_{eff} immediately gives the constant force, which is the plateau value.

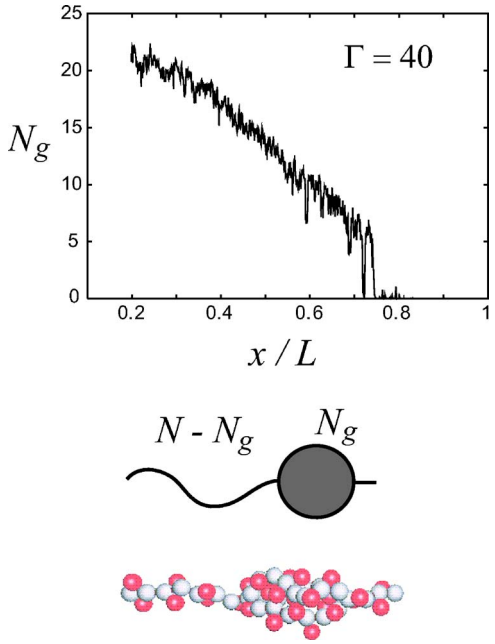

FIG. 5. (Color online) Top: the number of the monomers remaining in the globule, N_g, as a function of $x/\langle L\rangle$, under pulling with $\Gamma=40$. Bottom: snapshot of a PE with $\Gamma=40$ at the intermediate stage of pulling, exhibiting a ball-chain structure, together with its schematic illustration.

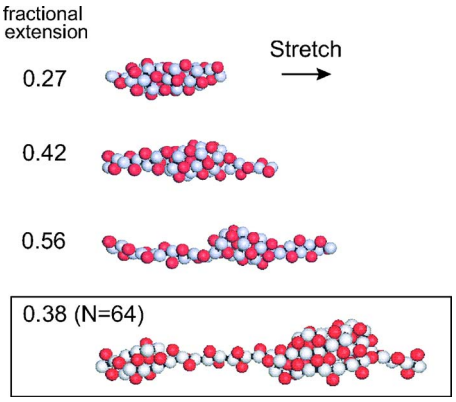

FIG. 6. (Color online) Snapshots of a PE during stretching for $\Gamma=110$. Corresponding f-x curve is Fig. 1(c). The ball-chain configuration is evident for a PE with $N=64$ monomers. Its force-extension curve is shown in Fig. 7(a).

VI. STICK-RELEASE PATTERN

In Fig. 1(c), we show the f-x curve for the largest coupling parameter $\Gamma=110$. The curve exhibits a pronounced sawtooth pattern, reflecting intermittent plastic deformations of the glasslike ionic condensate [17,52]. Figure 6 shows a series of the corresponding snapshots of the PE. The ball-chain configuration is most distinct for $N=64$. The f-x curve of PE with $N=64$ is also shown in Fig. 7, giving no qualitative difference with that of $N=32$. For a sufficiently large Γ, the electrostatic attractions are so strong that the PE cannot alter its intrachain conformation easily, because a significant energetic penalty should be imposed on the PE conformations in which the charge of any particle cannot be compensated immediately by its neighbors. The elastic energy is therefore more and more stored in the chain as the extension

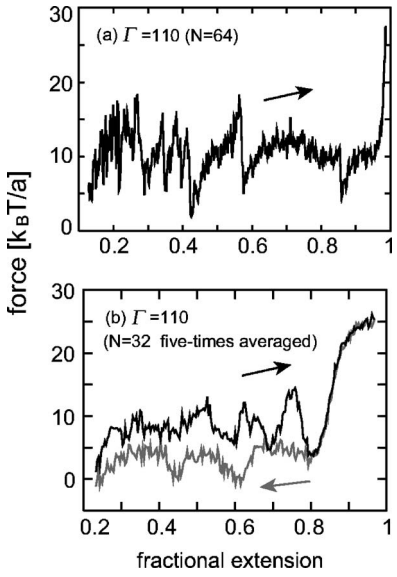

FIG. 7. (a) Force-extension curve of a PE with $N=64$ for $\Gamma=110$ in stretching. (b) The f-x curve averaged over the five independent runs with an identical initial state of a PE with $N=32$ for $\Gamma=110$.

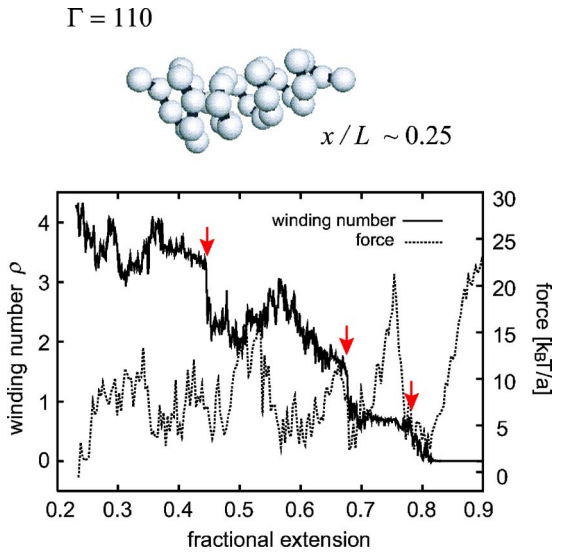

FIG. 8. (Color online) Top: snapshot of a PE condensate without surrounding counterions, which takes a helical configuration. Below: winding number ρ as a function of the fractional extension $x/\langle L\rangle$. Arrows highlight the points where the force drops involve one or half turn decrease of the winding number, ρ.

increases, until the PE condensate is locally unraveled over the strong dynamic electrofriction [61] in a rather abrupt way.

The reason why the stick-release-like pattern is obtained in our simulation is best understood in Fig. 8. In Fig. 8, a slightly stretched configuration of the condensed PE is shown without the surrounding counterions: The chain is winding around the stretching axis; i.e., it takes a helical structure. To see how this periodic structure in an intermediate scale is deformed as the PE is stretched, we monitored in Fig. 8 the change of the winding number ρ, which is defined by

$$\rho = \frac{1}{2\pi}\int_0^L \kappa(s)ds = \frac{1}{\pi}\sum_{j=1}^{N-2} |\tilde{\mathbf{u}}_{j+1} - \tilde{\mathbf{u}}_j|, \tag{9}$$

where s is the contour length of the chain from its one end, $\kappa(s)=|d^2\mathbf{r}(s)/ds^2|$ is the magnitude of the local curvature, and the summation is taken only for monomers whose centers are separated by distances larger than $3a$ from the stretching axis. This constraint is necessary to discriminate a "zigzag" state [45] from a "helical" state that we are focusing on. Figure 7 shows that corresponding to the sudden decrease of the tensile force, ρ is also decreased with one turn or half of a turn.

This finding might be positive with the expectation that the experimental stick-release pattern accompanies the turn-by-turn periodic unfoldings of a toroidal supercoiling. However, the present simulation does not confirm it because the number of PE monomers is very small, and thereby the granularity of each monomer can also play a non-negligible role in the appearance of the sawtooth pattern here.

The refolding behavior of a PE under relaxing is also studied for $\Gamma=110$. One can see marked hysteresis in the f-x curve [Fig. 1(c)]. This suggests that folding and unfolding transitions of the PE with its counterions are first-order-like [62]. The feature is more distinctive in Fig. 7(b), which shows the f-x curve averaged over the five independent runs with an identical initial state. The averaged curve is smoothed out compared to the single-pass curve in Fig. 1(c), confirming that each stick-release response is caused by a nonequilibrium conformational change of the PE. Averaging over a large number of single-pass f-x curves, one would obtain a smooth f-x curve with vanishing peaks. However, a hysteresis would remain even in that limit, as long as a time scale of v_s is faster than the longest transition time of a PE condensate to overcome an intramolecular local energy barrier [63].

VII. DISCUSSION

A. Counterion charge orderings

We now turn our attention to the counterion charge distribution to make clear the underlying mechanism behind the different types of PE elasticities. For a stretched PE, however, a distribution of condensed counterions becomes highly anisotropic; we thus cannot use the (angle-averaged) radial distribution function any more to characterize it. Instead, we consider here a highly stretched PE and investigate a one-dimensional (1D) counterion distribution along the PE backbone. In Fig. 9, the counterion pair distribution functions $g_{cc}(x)$ are shown for $\Gamma=40$ and 110, with the PE fractional extension u being kept nearly 0.9. Here $g_{cc}(x)$ is calculated according to

$$g_{cc}(x) = \frac{1}{N}\left\langle \sum_{i\neq j} \delta(x - x_i^c + x_j^c)\right\rangle, \tag{10}$$

where $x_i^c(t)$ is the x component of the ith counterion position and the brackets represent the long-time average (taken as roughly 10^7 time steps). To qualitatively discuss the observed structures of the counterions, we also show the 1D structure factor $S(q_\parallel)$ which is a direct Fourier transform of $g_{cc}(x)$. While $S(q_\parallel)$ has no particular structure for $\Gamma=40$ (which is similar to that of an ideal gas), there is a prominent peak at $q_\parallel a\sim\pi$ for $\Gamma=110$, which is identified as the Coulombic ground-state configuration of the condensed counterion. On the other hand, the self-diffusion of a counterion (averaged over all particle motions) is, although extremely slow, subdiffusive even for $\Gamma=110$. See Fig. 9(c). For both cases the values of Γ are much larger than 1; counterions form a moderately to strongly correlated liquid (as we have seen for the PE condensates). However, there still exist qualitative differences: For $\Gamma=40$, counterions highly fluctuate in the diffuse condensed layers and the fluctuating dipole (ionic-pair) interaction gives rise to net attraction between PE monomers [7–9,14,51,59]. The role of thermal fluctuations is therefore important here, and the PE globule may behave like an ionic droplet which could be easily deformed under an external pulling, giving a force plateau. On the other hand, for $\Gamma=110$, counterions are in a glasslike phase rather than in a usual liquid phase, with the short-range ionic-crystal order. This short-range order creates a very strong attraction be-

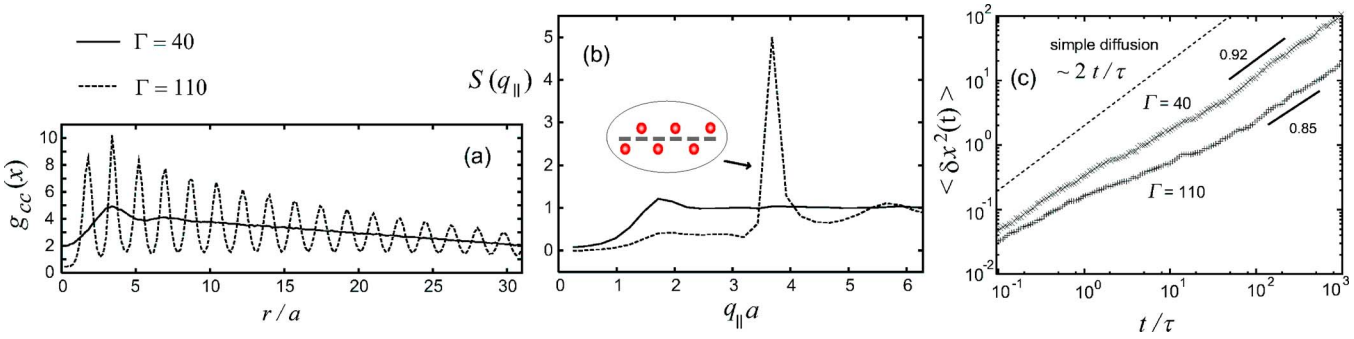

FIG. 9. (Color online) (a) 1D pair-distribution function, $g_{cc}(x)$, of counterions condensed onto a stretched PE with its fractional extension u being nearly 0.9, for $\Gamma=40$ (solid line) and for $\Gamma=110$ (dashed line). (b) 1D structure factor $S(q_{\|})$ of counterions, a direct Fourier transform of (a). (c) Self-diffusions of a single counterion for $\Gamma=40$ and 110, both of which exhibit subdiffusive behavior given, respectively, by $\langle \delta x^2(t) \rangle \propto t^z$ with $z=0.92$ for $\Gamma=40$ and with $z=0.85$ for $\Gamma=110$.

tween similarly charged objects, which may lead to the PE condensate having the stable periodic structure, combined with the bending rigidity of the PE chain. In this regime, dynamic unfolding behavior is observed as the stick-release pattern. This idea may also be supported by the prediction that, for much larger Γ (below the melting temperature), the latter attraction dominates over the former one at a very short distance that is typically the inter particle distance b [64,65]. In order to verify those, extensive data for larger-N systems will be required because we have to diminish finite-size effects and the influence of the system-size-dependent duration time of metastable states as much as possible.

B. Influence of the pulling rate: Effects of intrachain friction

Throughout the simulation, we have fixed the pulling speed v_s as $\alpha=v_s/v_0=0.1$. The unfolding behavior of a PE condensate is, however, known to be strongly pulling rate dependent. Figure 10 shows an example where two f-x curves for $\alpha=0.1$ and 4.0 are quite different. Also, the fluttering of the force becomes stronger as increasing the pulling speed. To qualitatively characterize the influence of the pulling speed on a force-extension curve, we plot in Fig. 10(b) the irreversible work ΔW [defined by Eq. (8)] for $\Gamma=60$, as a function of α. (Data for $\alpha>1$ are 3-times averaged due to large fluctuations of the force.) The excess work increases linearly with the pulling rate, following approximately the functional form $\Delta W/k_BT=1.95+0.85\alpha$, which is shown by a dashed line in Fig. 10(b). While the precise reason for this is at present unclear, the value we used ($\alpha=0.1$) is found to be in the convergent region, leading to the conclusion that the results presented in this paper are, at least, free from extreme pulling-rate-dependent effects. More detailed studies of the effects of the intramolecular friction [55,66] or a possible link to a Jarzinsky-type equation [67] will be reported elsewhere.

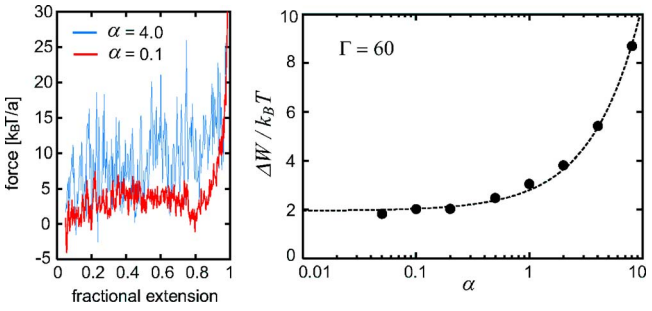

FIG. 10. (Color online) (a) Force-extension curves obtained for the pulling rate $\alpha=0.1$ (red) and $\alpha=4.0$ (blue), with $\Gamma=60$. (b) Excess work ΔW as a function of the pulling rate α for $\Gamma=60$. Data for $\alpha>1$ are 3-times averaged.

VIII. SUMMARY

In this paper, we have studied a strongly nonlinear regime of the elasticity of a single polyelectrolyte condensate by dynamic simulation in a wide range of the electrostatic coupling parameter Γ. The simulation results are apparently consistent with experimental trends. As the PE condensate takes a liquidlike to a solidlike structure, its force-extension curve crosses over from a force-plateau to a sawtooth response. We have provided a physical interpretation of these responses in terms of PE's conformational changes under stretching, together with their energetic stabilities against thermal fluctuations. Charge orderings of the condensed counterions have been investigated for both collapsed and stretched PE's, demonstrating the formation of moderately to strongly correlated liquid states. Especially in the limit of strong coupling, a short-range crystal-like order of counterions on the surface of the PE, which is compatible to recent strong-coupling theories [6,13,15–21,64,65], has been found. Simulations of larger-N systems, as well as incorporating hydrodynamic interactions, are currently in progress and will be reported elsewhere.

ACKNOWLEDGMENTS

We thank N. Yoshinaga, M. Wadati, M. Doi, H. Tanaka, A. Kitao, K. Kuwajima, M. Olvera de la Cruz, R. R. Netz, and A. A-Katz for useful discussions and comments. This work was supported by a Grant-in-Aid from JSPS.

[1] J. Israelachvili, *Intermolecular and Surface Forces*, 2nd ed. (Academic, London, 1992).
[2] R. M. Fuoss, A. K. Katchalsky, and S. Lifson, Proc. Natl. Acad. Sci. U.S.A. **37**, 579 (1951).
[3] F. Oosawa, Biopolymers **6**, 1633 (1968).
[4] L. Guldbrand, B. Jonsson, H. Wennerstrom, and P. Linse, J. Chem. Phys. **80**, 2221 (1984).
[5] R. Kjellander, S. Marcelja, R. M. Pashley, and J. P. Quirk, J. Chem. Phys. **92**, 4399 (1990).
[6] I. Rouzina and V. A. Bloomfield, J. Phys. Chem. **100**, 9977 (1996).
[7] N. Gronbech-Jensen, R. J. Mashl, R. F. Bruinsma, and W. M. Gelbart, Phys. Rev. Lett. **78**, 2477 (1997).
[8] B. Y. Ha and A. J. Liu, Phys. Rev. Lett. **79**, 1289 (1997).
[9] M. Deserno, A. Arnold, and C. Holm, Macromolecules **36**, 249 (2003).
[10] P. A. Pincus and S. A. Safran, Europhys. Lett. **42**, 103 (1998).
[11] Y. W. Kim and W. Sung, Europhys. Lett. **58**, 147 (2002).
[12] N. V. Brilliantov, D. V. Kuznetsov, and R. Klein, Phys. Rev. Lett. **81**, 1433 (1998).
[13] T. T. Nguyen, I. Rouzina, and B. I. Shklovskii, J. Chem. Phys. **112**, 2562 (2000).
[14] S. Liu and M. Muthukumar, J. Chem. Phys. **116**, 9975 (2002).
[15] B. I. Shklovskii, Phys. Rev. E **60**, 5802 (1999).
[16] J. J. Arenzon, J. F. Stlick, and Y. Levin, Eur. Phys. J. B **12**, 79 (1999).
[17] F. J. Solis and M. Olvera de la Cruz, J. Chem. Phys. **112**, 2030 (2000).
[18] R. R. Netz, Eur. Phys. J. E **5**, 557 (2001).
[19] A. G. Moreira and R. R. Netz, Phys. Rev. Lett. **87**, 078301 (2001).
[20] A. Naji and R. R. Netz, Eur. Phys. J. E **13**, 43 (2004).
[21] H. Frusawa, J. Phys. Soc. Jpn. **73**, 507 (2004).
[22] J. Widom and R. L. Baldwin, J. Mol. Biol. **144**, 431 (1980).
[23] G. E. Plum, P. G. Arscott, and V. A. Bloomfield, Biopolymers **30**, 619 (1990); **30**, 631 (1990).
[24] V. A. Bloomfield, Biopolymers **44**, 269 (1997).
[25] M. J. Stevens, Biophys. J. **80**, 130 (2001).
[26] See, for example, W. M. Gelbart, in *Electrostatic Effects in Soft Matter and Biophysics*, edited by C. Holm *et al.* (Kluwer, Dordrecht, 2001).
[27] T. E. Angelini, H. Liang, W. Wriggers, and G. C. Wong, Proc. Natl. Acad. Sci. U.S.A. **100**, 8634 (2003).
[28] J. C. Butler, T. Angelini, J. X. Tang, and G. C. L. Wong, Phys. Rev. Lett. **91**, 028301 (2003).
[29] R. Das, T. T. Mills, L. W. Kwok, G. S. Maskel, I. S. Millett, S. Doniach, K. D. Finkelstein, D. Herschlag, and L. Pollack, Phys. Rev. Lett. **90**, 188103 (2003).
[30] J. Skolnick and M. Fixman, Macromolecules **10**, 944 (1977).
[31] T. Odijk, J. Polym. Sci., Polym. Phys. Ed. **15**, 477 (1977).
[32] M. J. Stevens and K. Kremer, Phys. Rev. Lett. **71**, 2228 (1993); J. Chem. Phys. **103**, 1669 (1995).
[33] J.-L. Barrat and J.-F. Joanny, Europhys. Lett. **24**, 333 (1993); Adv. Chem. Phys. **94**, 1 (1996).
[34] R. R. Netz and H. Orland, Eur. Phys. J. B **8**, 81 (1999).
[35] C. G. Baumann, S. B. Smith, V. A. Bloomfield, and C. Bustamante, Proc. Natl. Acad. Sci. U.S.A. **94**, 1685 (1997).
[36] C. G. Baumann, V. A. Bloomfield, S. B. Smith, C. Bustamante, and M. D. Wang, Biophys. J. **78**, 1965 (2000).
[37] Y. Murayama and M. Sano, J. Phys. Soc. Jpn. **70**, 345 (2001).
[38] Y. Murayama, Y. Sakamaki, and M. Sano, Phys. Rev. Lett. **90**, 018102 (2003).
[39] J. F. Marko and E. D. Siggia, Macromolecules **28**, 8759 (1995).
[40] A. Halperin and E. B. Zhulina, Europhys. Lett. **15**, 417 (1991).
[41] I. M. Kulic and H. Schiessel, Phys. Rev. Lett. **92**, 228101 (2004).
[42] M. N. Tamashiro and H. Schiessel, Macromolecules **33**, 5263 (2000).
[43] H. J. Limbach, C. Holm, and K. Kremer, Europhys. Lett. **60**, 566 (2002).
[44] M. O. Khan and D. Y. C. Chan, J. Phys. Chem. B **107**, 8131 (2003); Macromolecules **38**, 3017 (2005).
[45] D. Marenduzzo, A. Martian, and A. Rose, Eur. Phys. J. E **15**, 83 (2004).
[46] N. Yoshinaga, K. Yoshikawa, and T. Ohta, e-print cond-mat/0410226.
[47] Y. Murayama and M. Sano, Biopolymers **77**, 354 (2005).
[48] E. Allahyarov, G. Gompper, and H. Lowen, Phys. Rev. E **69**, 041904 (2004).
[49] D. J. Adams and G. S. Dubey, J. Comput. Phys. **72**, 156 (1987).
[50] J. Lekner, Physica A **176**, 485 (1991).
[51] R. G. Winkler, M. Gold, and P. Reineker, Phys. Rev. Lett. **80**, 3731 (1998).
[52] R. G. Winkler, M. O. Steinhauser, and P. Reineker, Phys. Rev. E **66**, 021802 (2002).
[53] R. R. Netz, Phys. Rev. Lett. **90**, 128104 (2003); J. Phys. Chem. B **107**, 8209 (2003).
[54] M. Doi and S. F. Edwards, *The Theory of Polymer Dynamics* (Oxford University Press, Oxford, 1986).
[55] P. G. de Gennes, *Scaling Concepts in Polymer Physics* (Cornell University Press, Ithaca, 1979).
[56] V. A. Ivanov, W. Paul, and K. Binder, J. Chem. Phys. **109**, 5659 (1998).
[57] H. Noguchi and K. Yoshikawa, J. Chem. Phys. **113**, 854 (2000).
[58] G. S. Manning, Q. Rev. Biophys. **2**, 179 (1978).
[59] R. Golestanian and T. B. Liverpool, Phys. Rev. E **66**, 051802 (2002).
[60] R. Zhang and B. I. Shklovskii, Physica A **349**, 563 (2005).
[61] R. R. Netz, Phys. Rev. Lett. **91**, 138101 (2003).
[62] I. R. Cooke and D. R. M. Williams, Europhys. Lett. **64**, 267 (2003).
[63] H. Wada, Y. Murayama, and M. Sano, Phys. Rev. E **66**, 061912 (2002).
[64] F. J. Solis and M. Olvera de la Cruz, Phys. Rev. E **60**, 4496 (1999).
[65] A. W. C. Lau, P. Pincus, D. Levine, and H. A. Fertig, Phys. Rev. E **63**, 051604 (2001).
[66] M. G. Poirier and J. F. Marko, Phys. Rev. Lett. **88**, 228103 (2002).
[67] J. Liphartdt, S. Dumont, S. B. Smith, I. Tinoco, and C. Bustamante, Science **296**, 1832 (2002).